# An Adaptive Fast Terminal Sliding Mode and ADRC Fusion Control for Quadcopter UAVs

Jianfeng Che
*School of Engineering*
*Taylor's University*
Selangor, Malaysia
0363052@sd.taylors.edu.my

Swee King Phang
*School of Engineering*
*Taylor's University*
Selangor, Malaysia
sweeking.phang@taylors.edu.my

Lin Ge
*School of Engineering*
*Taylor's University*
Selangor, Malaysia
lin.ge@sd.taylors.edu.my

*Abstract*—**This research addresses the complexities through the development of an innovative control strategy that merges adaptive Fast Terminal Sliding Mode Control with linear Active Disturbance Rejection Control (AFTSMC-ADRC). To enhance UAV performance in the presence of external disturbances and model uncertainties, an adaptive convergence law is formulated. The control methodology entails the design of a rapid terminal sliding mode surface to facilitate global fast convergence, coupled with adaptive combination laws to amplify state convergence speed and robustness against disturbances. The efficacy of the proposed controller is empirically substantiated through practical flight experiments and simulation tests, revealing notable improvements in UAV tracking precision and resilience compared to conventional cascaded PID algorithms.**

*Keywords—UAV, Aerial Mapping, Map Reconstruction*

## I. INTRODUCTION

Unmanned Aerial Vehicle (UAV) is an aircraft capable of autonomously executing flight missions without needing professional flight personnel [1]. Unlike conventional aircraft, UAVs are smaller and more maneuverable, allowing them to complete complex flight tasks in dynamic environments through their autonomous control systems. They have been effectively employed in the field of logistics transportation [2], detection of marine fauna [3], assessment of habitat destruction [4], monitoring of crops [5], and mapping of buildings [6]. In addition, drone mapping has found extensive applications across diverse industries such as construction, agriculture, mining, and infrastructure inspection [7].

A quadcopter UAV represents an underactuated system with four control inputs but six degree-of-freedom (6-DOF) in its outputs [8], [9]. Moreover, UAVs are susceptible to uncertainties and disturbances during flight [10], [11], such as gusts of wind encountered during flight [12] or the addition of extra payloads [13]. These factors collectively pose significant challenges in designing effective control strategies for UAVs.

The aforementioned methods have made significant strides in addressing control challenges faced by quadcopter UAVs under uncertain conditions. However, certain limitations persist. The application of sliding mode control algorithms in the flight of quadcopter UAVs can induce undesirable vibrations, particularly in the presence of external disturbances. Likewise, the active disturbance rejection control algorithm has limitations in its estimation capabilities. Furthermore, adaptive control algorithms pose challenges in regulating speed, with rapid adjustments

leading to high feedback gains that compromise system robustness and slow adjustments elongating transient processes and reducing convergence rates. These issues collectively result in the suboptimal performance of UAVs in practical control scenarios.

In this article, considering external disturbances and model uncertainties, an adaptive fast terminal sliding mode control ADRC controller (AFTSMC-ESO) is designed. First, to achieve global fast convergence, a fast terminal sliding mode surface is designed to ensure rapid convergence of the system state when it deviates from the equilibrium point. Then, a combination of adaptive combination approach laws is designed to improve the convergence speed of the system state and its robustness to disturbances. Finally, the total disturbance estimated by the extended state observer is introduced into the design of the switching function, reducing the sliding mode chattering phenomenon caused by external disturbances. Experimental results demonstrate that the designed controller improves the tracking performance and robustness of the drone.

The motion model of the UAV will be presented in Section II of this article; the control algorithm designed in this article will be described in detail in Section III, the flight test of the designed control algorithm will be presented in Section IV; and finally, the concluding remarks will be presented in Section V.

## II. DYNAMIC MODEL OF QUADROTOR

To achieve optimal controller performance, it is imperative to establish a highly accurate mathematical model of the quadrotor. This section is to provide a comprehensive 6-DOF dynamic model of the quadrotor, which will serve as a valuable tool for controller design.
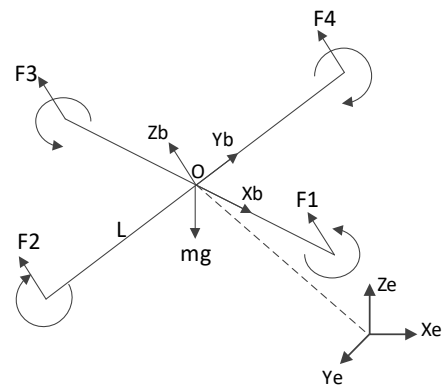


Fig. 1. The structure of the quadrotor.

In order to establish a quadrotor dynamic model, we first need to establish a suitable coordinate system. As shown in Fig. 1, $E = \{x_e, y_e, z_e\}$ denote the inertial coordinates used to describe the position of a quadrotor in space. $B = \{x_b, y_b, z_b\}$ denote the body fixed coordinates used to describe the attitude in the air. The absolute translational position of the aircraft is described by $\xi = \{x, y, z\}$, and its attitude by the Euler angles $\beta = [\varphi, \theta, \psi]$. Assuming that quadrotors are considered rigid bodies and the structure is symmetrical and the center of gravity coincides with the origin of the frame. The four control inputs can be defined as

$$\begin{cases} u_1 = F_1 + F_2 + F_3 + F_4 \\ u_2 = L(F_4 - F_2) \\ u_3 = L(F_3 - F_1) \\ u_4 = M_2 + M_4 - M_1 - M_3 \end{cases} \quad (1)$$

Where $L$ is the length from the rotor to the center of the mass of the quadrotor, is the generated thrust, and is the generated torque.

$$\begin{cases} \sum F = m(\dot{v} + \dot{\omega} \times v) \\ \sum N = I\dot{\omega} + \omega \times (I\dot{\omega}) \end{cases} \quad (2)$$

In the equation, $F$ is the combined external force on the wing of the UAV, $m$ is the mass of the UAV, $v = [u, v, w]$ is linear speed of the flight, $\omega = [p, q, r]$ is the angular velocity in the coordinate system of the fuselage, $N$ is the combined external moment acting on the UAV, $I$ is the moment of inertia.

Equation (2) can be rewritten as:

$$\begin{bmatrix} m_e & 0 \\ 0 & I \end{bmatrix} \begin{bmatrix} \dot{v} \\ \dot{\omega} \end{bmatrix} = \begin{bmatrix} f \\ N \end{bmatrix} - \begin{bmatrix} 0 \\ \omega \times I\omega \end{bmatrix} \quad (3)$$

Equations governing dynamics of the quadrotor with respect to the inertial coordinates are generally expressed as

$$\begin{cases} \ddot{x} = (\sin\theta \cos\phi \cos\psi + \sin\phi \sin\psi)\frac{u_1}{m} + d_x \\ \ddot{y} = (\sin\theta \cos\phi \cos\psi - \sin\phi \sin\psi)\frac{u_1}{m} + d_y \\ \ddot{z} = \cos\phi \cos\theta \frac{u_1}{m} - g + d_z \\ \ddot{\phi} = \frac{1}{I_{xx}}\left((I_{yy} - I_{zz})\dot{\theta}\dot{\psi} + u_2\right) + d_\phi \\ \ddot{\theta} = \frac{1}{I_{yy}}\left((I_{zz} - I_{xx})\dot{\phi}\dot{\psi} + u_3\right) + d_\theta \\ \ddot{\psi} = \frac{1}{I_{zz}}\left((I_{xx} - I_{yy})\dot{\phi}\dot{\theta} + u_4\right) + d_\psi \end{cases} \quad (4)$$

## III. CONTROLLER DESIGN
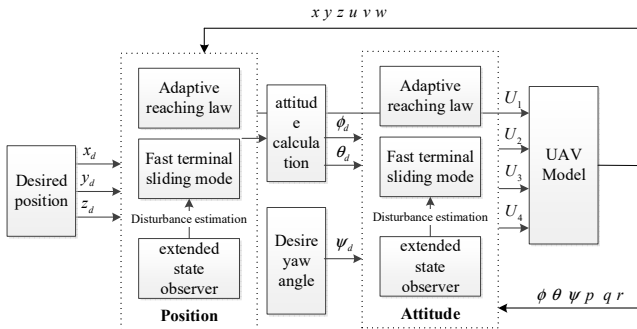


Fig. 2. The structure of the quadrotor.

### A. Position Controller

This section primarily focuses on the design of an adaptive fast terminal sliding mode controller to meet the requirement for rapid tracking performance in quadcopter UAVs. Within the position control system, there is no coupling relationship among the three position outputs, allowing for the design of individual controllers for each. Below, we illustrate the controller structure with the altitude channel as an example. The fig.2 show the structure of the quadrotor.

The designed non-singular rapid termination sliding mode surface is

$$s_1 = e_1 + \alpha_1 |e_1|^{a_1} sgn\, e_1 + \beta_1 |\dot{e}_1|^{b_1} sgn\, e_1 \quad (5)$$

where sliding mode parameter, $\alpha_1 > 0$, $\beta_1 > 0$, $1 < b_1 < 2$, $a_1 > b_1$.

By integrating the quadcopter model with the ESO, the equation governing the state of the altitude channel can be simplified as follows:

$$\begin{cases} \dot{z}_1 = z_2 \\ \dot{z}_2 = \hat{z}_3 + u_z \end{cases} \quad (6)$$

Where $z_1$ and $z_2$ are the actual altitude and derivative values of the quadcopter UAV; $\hat{z}_3$ the total disturbance value estimated by the ESO。

Define the error variables:

$$\begin{cases} e_1 = z_d - z_1 \\ \dot{e}_1 = \dot{z}_d - \dot{z}_1 \\ \ddot{e}_1 = \ddot{z}_d - \hat{z}_3 - u_z \end{cases} \quad (7)$$

Combining formulas (6)-(7) the sliding mode function derivative is:

$$\begin{aligned} \dot{s}_1 = \dot{e}_1 + \alpha_1 a_1 |e_1|^{a_1-1}\dot{e}_1 \\ + \beta_1 b_1 |\dot{e}_1|^{b_1-1}(\ddot{z}_d - \hat{z}_3 - u_x) \end{aligned} \quad (8)$$

To address the problem that sliding mode controllers are usually susceptible to external perturbations during the arrival phase, a combined adaptive convergence law is used to ensure the controller performance and suppress jitter in the following form:

$$\dot{s}_1 = -\omega_1 s_1 - \lambda_1 |s_1|^{\gamma_1} sgn(s_1) - v(s_1)\, sgn(s_1) \quad (9)$$

Where $\omega_1, \lambda_1, \gamma_1$ are control parameters, $0 < \gamma_1 < 1$; $v(s_1)$ denotes the adaptive gain in the following form:

$$\begin{cases} \dot{v}(x) = l_1|x| - l_2 v(x) \\ v = v_{max} sat(v/v_{max}) \end{cases} \quad (10)$$

Where is the gain parameter, $v_{max}$ denotes the maximum value of $v(s)$; $sat(\cdot)$ is the saturation function of the following form:

$$sat\left(\frac{v}{v_{max}}\right) = \begin{cases} 1, & v \geq v_{max} \\ \frac{v}{v_{max}}, & v < v_{max} \end{cases} \quad (11)$$

Combining Eqs. (8) and (9) gives the virtual control rate of the height channel as:

2

$$u_z = \ddot{z}_d - \hat{z}_3 + \frac{1}{\beta_1 b_1 |\dot{e}_1|^{b_1-1}}(\dot{e}_1 + \alpha_1 a_1 |e_1|^{a_1-1}\dot{e}_1)$$
$$- \omega_1 s_1 - \lambda_1 |s_1|^{\gamma_1} \operatorname{sgn}(s_1) - v(s_1)\operatorname{sgn}(s_1) \quad (12)$$

### B. Attitude Controllers

In this section, the quadrotor attitude controller is designed based on the desired yaw angle setpoint and the pitch and roll angle setpoints solved by the position loop. The roll angle channel is still used as an example to illustrate the controller structure.

The attitude controller design method is similar to the position controller, and the fast terminal sliding mode function is designed as:

$$s_4 = e_4 + \alpha_4 |e_4|^{a_4} \operatorname{sgn} e_4 + \beta_4 |\dot{e}_4|^{b_4} \operatorname{sgn} \dot{e}_4 \quad (13)$$

The adaptive convergence rate is:

$$\dot{s}_4 = -\omega_4 s_4 - \lambda_4 |s_4|^{\gamma_4} \operatorname{sgn}(s_4) - v(s_4)\operatorname{sgn}(s_4) \quad (14)$$

Combining Eqs. (13)-(14) gives the roll channel control rate as:

$$u_2 = \frac{1}{b_1}\begin{pmatrix} \ddot{\phi}_d - \hat{\phi}_3 + \frac{1}{\alpha_4 a_4 |\dot{e}_4|^{a_4-1}}(\dot{e}_4 + \beta_4 b_4 |e_4|^{c_4-1}\dot{e}_4) \\ -\omega_4 s_4 - \beta_4 |s_4|^{\gamma_4}\operatorname{sgn}(s_4) - v(s_4)\operatorname{sgn}(s_4) \end{pmatrix}$$

### C. Stability analysis

Next, a convergence analysis of a closed-loop quadrotor UAV system based on an adaptive fast terminal sliding mode controller is performed.

$$V = V_S + V_{ESO} \quad (15)$$

For the adaptive fast terminal sliding mode control part, the Lyapunov function is chosen:

$$V_s = \frac{1}{2} s_i^2 \quad (16)$$

Combining the first order, derivatives of $V_i$ the above equation is:

$$\dot{V}_s = s_i \cdot \dot{s}_i = -\sigma_i s_i^2 - \sigma_j |s_i|^{\gamma_i+1} - v(s_i)|s_i| \quad (17)$$

As $0 \le v(s_i) \le v(s_i)_{\max}$,

$$\dot{V}_s = -\sigma_i s_i^2 - \sigma_j |s_i|^{\gamma_i+1} - v(s_i)|s_i| \le 0 \quad (18)$$

$$V_{ESO}(t) = \eta^T P \eta \quad (19)$$

The derivative $V_{ESO}$ is

$$\dot{V}_{ESO}(t) = \dot{\eta}^T P \eta + \eta^T P \dot{\eta}$$
$$= \left(\frac{1}{r}A_\eta \eta + B\dot{f}(t)\right)^T P\eta + \eta^T P\left(\frac{1}{r}A_\eta \eta + B\dot{f}(t)\right)$$
$$= -\frac{1}{r}\eta^T Q\eta + 2\dot{f}(t)B^T P\eta$$
$$\le -\frac{1}{r}\lambda\|\eta\|^2 \|B^T P\|\|\eta\|_{min} \quad (20)$$

where $\lambda_{min}$ is the minimum eigenvalue of the matrix and is the maximum value of $\dot{f}(t)$.

$$\|\eta\| \le \frac{2nr\|B^T P\|}{\lambda_{min}}, \quad \dot{V}_{ESO}(t) \le 0 \quad (21)$$

Combines three attitude channels and three position channels：

$$\dot{V} = \sum_{i=1}^{6} V_{ESOi} + V_{si} \le 0 \quad (22)$$

Therefore, combining the above equation can be, quadcopter UAV control closed loop Lyapunov stabilization.

### IV. FLIGHT TESTING RESULTS

To verify the effectiveness of the control algorithms designed in this chapter, the attitude control is verified by indoor flight on the Hummingbird UAV, and the position control is verified by simulation on the MATLAB/Simulink software.

The indoor flight experiments include attitude tracking experiments under undisturbed conditions and anti-disturbance experiments under wind and load disturbances.

### A. Flight Testing platforms

A testing platform for the validation of designed algorithms has been constructed. The overall structure of the indoor test platform is illustrated in the diagram, consisting of a quadcopter, a remote controller, a ground station, and a wireless data transmission module Xbee. The remote controller is used to send control commands to the quadcopter, which responds by making corresponding attitude changes. The sensor data is transmitted in real-time to the ground station through the Xbee wireless data transmission module. In addition to receiving data, the ground station can also send parameters to the quadcopter using the Xbee module is given in Fig 3.
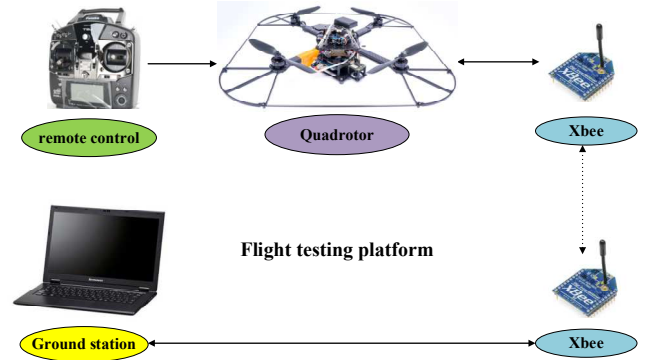


Fig. 3. Flight testing platform.

The indoor flight testing takes place in an indoor environment with approximate dimensions of 2.5×2.5×3m. To ensure the safety of the experimental equipment, the testing is conducted on a safety net with a mesh size of 12×12 cm, protecting against the potential crash of the quadrotor. Additionally, a safety mat is placed on the bottom to further safeguard against any impact from quadrotor falls.

### B. Wind Resistance Testing

To create gust effects, a desktop fan was placed in one corner of the experimental net as shown in Fig. 4(a). The experiment lasted for 50 seconds, with the fan being turned on and blowing towards the quadcopter at the 5th second, and turned off at the 45th second. The aim was to observe the

3

attitude control effect of the quadcopter at this time. To quantify the wind speed, a handheld anemometer was used to measure the fan's wind speed. The measured wind speed is shown in Fig. 4(b).

To validate the effectiveness of the control algorithm designed in this chapter, a comparison is conducted between the algorithm designed in this chapter and the cascaded PID algorithm. The actual attitude changes are shown in Fig. 5 and 6. Table 1 shows the performance comparison of the two algorithms.



(a)                            (b)
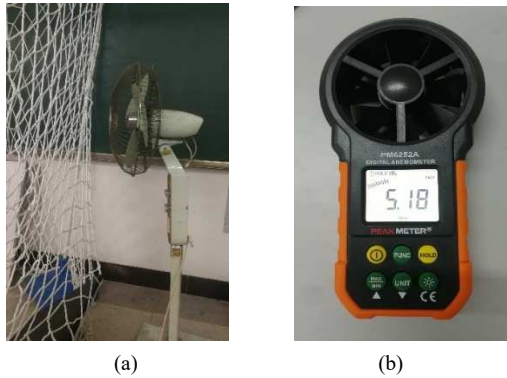
Fig. 4.   (a) Vertical electric fan; (b) Handheld anemometer results.
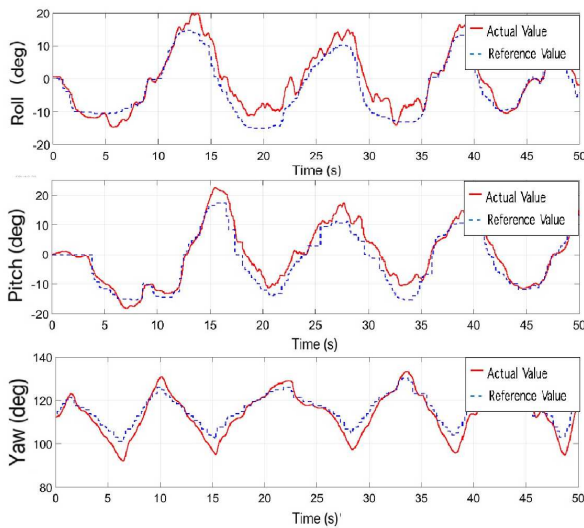


Fig. 5.   UAV Wind-resistant attitude profile based on Cascaded PID.
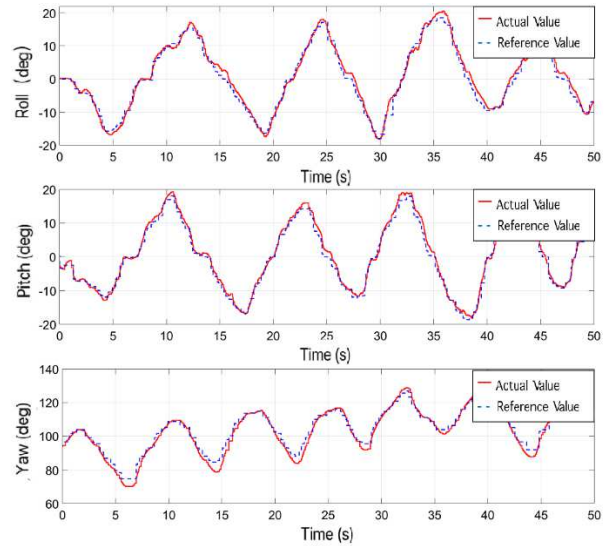


Fig. 6.   UAV Wind-resistant attitude profile based on AFTSMC-ESO.

## C. Actual UAV Experimental Footage

In practical operations, quadcopters often need to carry application devices. However, the additional payload attached to the drone will alter its weight. Additionally, during flight, the attached payload may cause oscillations due to changes in flight attitude, thereby affecting the drone's center of gravity. This part will conduct a load experiment to compare the anti-interference capabilities of the designed algorithm with cascaded PID. The specific experimental steps are as follows: a bottle weighing 80 g is tied to the center of the drone's bottom using a 30cm nylon rope, as shown in Fig. 7. The drone is then remotely controlled to take off with the water bottle attached, and control commands are sent through the remote controller to the three attitude channels. Fig. 8 and Fig. 9 show the actual attitude changes of the two algorithms, while Table 2 shows the performance differences between the two algorithms.

TABLE I.        COMPARISON OF WIND RESISTANCE PERFORMANCE

| Channel | Control methods | Tolerance range/(°) | Maximum overshoot/(°) |
|---|---|---|---|
| Roll | AFTSMC-ESO | -3.8~5.4 | 27.1% |
|  | Cascaded PID | -4.7~9.5 | 42.6% |
| Pitch | AFTSMC-ESO | -5.9~4.4 | 28..2% |
|  | Cascaded PID | -4.3~9.2 | 41.8% |
| Yaw | AFTSMC-ESO | -7.4~5.0 | 8.3% |
|  | Cascaded PID | -14.8~10.8 | 14.2 |

4

Fig. 7. Drone load disturbance test diagram
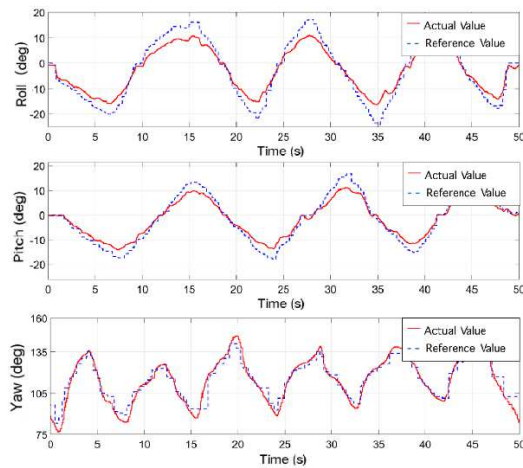


Fig. 8. UAV Load Attitude Profile Based on Cascaded PID
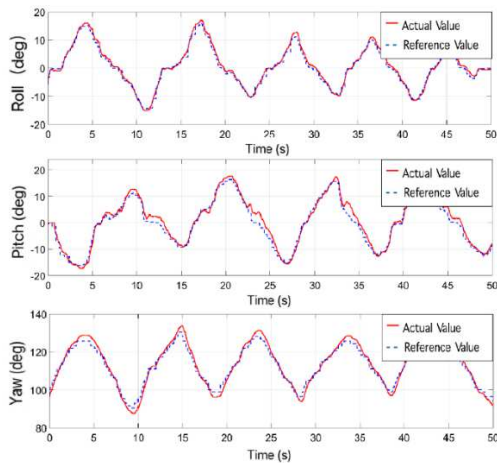


Fig. 9. UAV Load Attitude Profile Based on AFTSMC-ESO

TABLE II. LOAD PERFORMANCE COMPARISON

| Channel | Control methods | Tolerance range/(°) | Maximum overshoot/(°) |
|---|---|---|---|
| Roll | AFTSMC-ESO | -3.8~5.4 | 23.1% |
| | Cascaded PID | -4.7~9.2 | 42.6% |
| Pitch | AFTSMC-ESO | -5.9~4.4 | 23..2% |
| | Cascaded PID | -6.8~7.2 | 41.8% |
| Yaw | AFTSMC-ESO | -7.4~5.0 | 6.0% |
| | Cascaded PID | -19.3~23.1 | 13.4% |

*D. Position Simulation testing*

In this section, the Simulink tool is used to verify the superiority of the dynamic non-singular fast terminal sliding mode self-resistant controller proposed in this paper, and the algorithm is compared with the conventional sliding mode controller during the simulation process, where AFTSMC+ESO denotes the proposed control method and SMC denotes the conventional control method. The initial position and attitude angle values of the quadrotor UAV tested in the simulation are $[0,0,0]rad$, The desired trajectory of the trace $\left[cos(\frac{t}{4}), sin(\frac{t}{4}), 1\right]$. In addition, in order to simulate the parameter uncertainty of the system, the actual model parameters of the system are randomly taken in the range of $0.7 \sim 1.3$ times the standard model parameters, and to simulate the system being subjected to the external perturbation, an external perturbation is applied, and the value of the external perturbation is. The results are shown below.
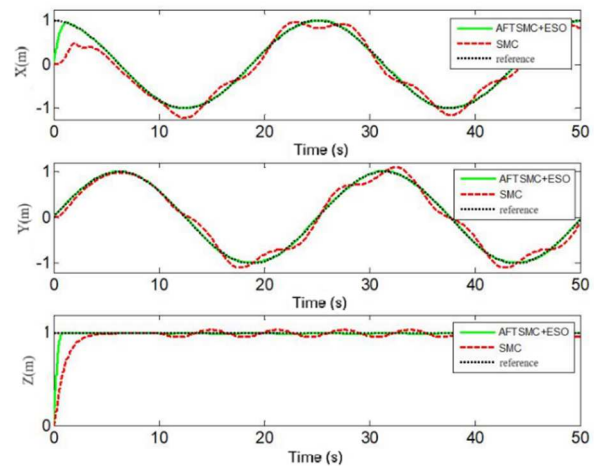


Fig. 10. UAV Position trajectory tracking graph

5
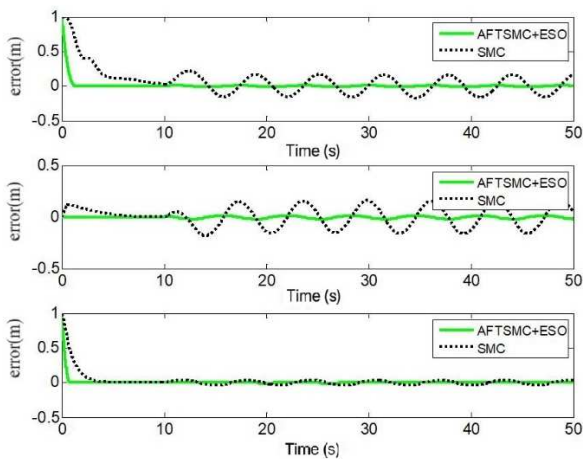
Fig. 11. UAV Position tracking error graph

Fig. 10 and Fig. 11 show the variation of position tracking error, in the 10 s before the introduction of perturbation the controller designed in this chapter can guarantee to track to the set value within 2 seconds, the rapidity is improved compared with the traditional sliding mode control and the error is 0. After 10 seconds of introducing the perturbation, the controller designed in this chapter can still guarantee to track to the set trajectory and the error is not greater than 0.05. While the traditional sliding mode control in the traditional sliding mode control is not able to suppress the perturbation well after adding the perturbation, and the error begins to vary with the perturbation to different degrees and in a wide range, the comparison proves that the proposed strategy has excellent perturbation capability.

## V. Conclusion

This article addresses control challenges related to external disturbances and model uncertainties in UAVs by introducing a control strategy that combines fast terminal non-singular sliding mode control with linear ADRC. An adaptive convergence law is designed to compensate for external disturbances, thereby enhancing the system's robustness against disturbances. Through practical flight experiments and simulation tests, the proposed control algorithm demonstrates significant performance improvements when compared to a cascaded PID algorithm. Experimental results validate that the designed controller further enhances the UAV's tracking performance and robustness.

## References

[1] S. K. Phang, C. Cai, B. M. Chen, and T. H. Lee, "Design and mathematical modeling of a 4-standard-propeller (4SP) quadrotor,"

in *Proceedings of the 10th World Congress on Intelligent Control and Automation*, IEEE, Jul. 2012, pp. 3270–3275. doi: 10.1109/WCICA.2012.6358437.

[2] H. Zhang *et al.*, "A Logistics UAV Parcel-Receiving Station and Public Air-Route Planning Method Based on Bi-Layer Optimization," *Applied Sciences*, vol. 13, no. 3, p. 1842, Jan. 2023, doi: 10.3390/app13031842.

[3] L. Goddijn-Murphy, B. J. Williamson, J. McIlvenny, and P. Corradi, "Using a UAV Thermal Infrared Camera for Monitoring Floating Marine Plastic Litter," *Remote Sens (Basel)*, vol. 14, no. 13, p. 3179, Jul. 2022, doi: 10.3390/rs14133179.

[4] C. Cruz, J. O'Connell, K. McGuinness, J. R. Martin, P. M. Perrin, and J. Connolly, "Assessing the effectiveness of UAV data for accurate coastal dune habitat mapping," *Eur J Remote Sens*, vol. 56, no. 1, Dec. 2023, doi: 10.1080/22797254.2023.2191870.

[5] M. Günder, F. R. Ispizua Yamati, J. Kierdorf, R. Roscher, A.-K. Mahlein, and C. Bauckhage, "Agricultural plant cataloging and establishment of a data framework from UAV-based crop images by computer vision," *Gigascience*, vol. 11, Jun. 2022, doi: 10.1093/gigascience/giac054.

[6] Y. Tan, G. Li, R. Cai, J. Ma, and M. Wang, "Mapping and modelling defect data from UAV captured images to BIM for building external wall inspection," *Autom Constr*, vol. 139, p. 104284, Jul. 2022, doi: 10.1016/j.autcon.2022.104284.

[7] H. Tan, W. Zheng, and P. Vijayakumar, "Secure and Efficient Authenticated Key Management Scheme for UAV-Assisted Infrastructure-Less IoVs," *IEEE Transactions on Intelligent Transportation Systems*, vol. 24, no. 6, pp. 6389–6400, Jun. 2023, doi: 10.1109/TITS.2023.3252082.

[8] S. K. Phang, K. Li, F. Wang, B. M. Chen, and T. H. Lee, "Explicit model identification and control of a micro aerial vehicle," in *2014 International Conference on Unmanned Aircraft Systems (ICUAS)*, IEEE, May 2014, pp. 1048–1054. doi: 10.1109/ICUAS.2014.6842356.

[9] J. J. Tai, S. K. Phang, and C. L. Hoo, "Application of Steady-State Integral Proportional Integral Controller for Inner Dynamics Control Loop of Multi-rotor UAVs," in *2018 Fourth International Conference on Advances in Computing, Communication & Automation (ICACCA)*, IEEE, Oct. 2018, pp. 1–6. doi: 10.1109/ICACCAF.2018.8776780.

[10] F. Pollet, M. Budinger, S. Delbecq, J.-M. Moschetta, and J. Liscouët, "Quantifying and mitigating uncertainties in design optimization including off-the-shelf components: Application to an electric multirotor UAV," *Aerosp Sci Technol*, vol. 136, p. 108179, May 2023, doi: 10.1016/j.ast.2023.108179.

[11] S. K. Phang, S. Zeeshan Ahmed, and M. R. Abdul Hamid, "Design, Dynamics Modelling and Control of a H-Shape Multi-rotor System for Indoor Navigation," in *2019 1st International Conference on Unmanned Vehicle Systems-Oman (UVS)*, IEEE, Feb. 2019, pp. 1–6. doi: 10.1109/UVS.2019.8658354.

[12] S. Li, Z. Sun, and M. A. Talpur, "A finite time composite control method for quadrotor UAV with wind disturbance rejection," *Computers and Electrical Engineering*, vol. 103, p. 108299, Oct. 2022, doi: 10.1016/j.compeleceng.2022.108299.

[13] Y.-H. Su, P. Bhowmick, and A. Lanzon, "A robust adaptive formation control methodology for networked multi-UAV systems with applications to cooperative payload transportation," *Control Eng Pract*, vol. 138, p. 105608, Sep. 2023, doi: 10.1016/j.conengprac.2023.105608.